AGU PUBLICATIONS

Geophysical Research Letters

RESEARCH LETTER
10.1002/2016GL071451

Key Points:
- The number of extremely strong front has increased over Europe, and the trend is tied to an increase in humidity (ERA-Interim 1979–2014)
- No trend in the number of extremely strong fronts is identified over North America
- Frontal precipitation rates increase with frontal strength

Supporting Information:
- Supporting Information S1

Correspondence to:
S. Schemm,
sebastian.schemm@uib.no

Citation:
Schemm, S., M. Sprenger, O. Martius, H. Wernli, and M. Zimmer (2017), Increase in the number of extremely strong fronts over Europe? A study based on ERA-Interim reanalysis (1979–2014), *Geophys. Res. Lett.*, *44*, 553–561, doi:10.1002/2016GL071451.

Received 3 OCT 2016
Accepted 30 NOV 2016
Accepted article online 5 DEC 2016
Published online 12 JAN 2017

Increase in the number of extremely strong fronts over Europe? A study based on ERA-Interim reanalysis (1979–2014)

S. Schemm[1,2], M. Sprenger[2], O. Martius[3], H. Wernli[2], and M. Zimmer[4]

[1]Geophysical Institute and Bjerknes Centre for Climate Research, University of Bergen, Bergen, Norway, [2]Institute for Atmospheric and Climate Science, ETH Zürich, Zürich, Switzerland, [3]Institute of Geography, Oeschger Centre, University of Bern, Bern, Switzerland, [4]State Environmental Agency Rhineland-Palatinate, Mainz, Germany

Abstract Evidence is presented that the frequency of extremely strong fronts, which occur mainly in summer, has increased over Europe in ERA-Interim reanalyses data (1979–2014). Fronts are defined using a common detection scheme based on gradients of equivalent potential temperature (θ_e) at 850 hPa. The frequency increase is due to increasing atmospheric humidity, which in turn is reported as statistically significant over Europe in the Fifth Assessment Report of the Intergovernmental Panel on Climate Change (IPCC AR5). There is no trend in the frequency of extremely strong fronts in North America where humidity trends are, according to the IPCC AR5, close to zero. Because frontal precipitation increases with frontal strength, measured by the θ_e gradient, the increase in the number of extremely strong fronts may help explain regional patterns of longer-term trends in strong precipitation events.

1. Introduction

High-impact, small-scale weather events, such as hail storms, wind extremes, or intense precipitation, are frequently associated with the passage of large-scale fronts [*James and Browning*, 1979; *Volkert et al.*, 1987; *Mills*, 2005; *Catto et al.*, 2012; *Catto and Pfahl*, 2013; *Reeder et al.*, 2015; *Schemm et al.*, 2016]. Hence, trends in the frequency, intensity, and spatial variability of fronts potentially are an important agent of trends in extreme weather phenomena and drivers behind their high spatiotemporal variability. In fact, *Catto and Pfahl* [2013] found that up to 90% of all midlatitude precipitation extremes are associated with fronts. They also showed that fronts that produce extreme precipitation events have on average higher frontal strengths by up to 35% (the front definition is discussed below). Consequently, it is not only the number of fronts that relates to the occurrence of extreme weather events but also their strength. Stronger fronts are more likely to be linked to extreme weather than weak fronts.

A front is related to a sharp transition in time or space of a relevant meteorological variable, e.g., density, temperature, humidity, or wind direction. The pertinent meteorological characteristic of a front is its horizontal gradient, which in this study we take as the gradient of equivalent potential temperature (θ_e) at the 850 hPa level. This choice is equivalent to *Catto and Pfahl* [2013] who used wet-bulb potential temperature on 850 hPa. Both these temperature combine the effects of strong temperature and humidity contrasts across the front, which is ideal for detecting cold and warm fronts and is a common and accepted technique to detect large-scale mobile fronts [*Hewson*, 1998; *Jenkner et al.*, 2010; *Hewson and Titley*, 2010; *Berry et al.*, 2011; *Schemm et al.*, 2015]. We justify our choice in greater detail in the methods section.

Research on weather extremes and their global and regional trends in a warmer and moister atmosphere have received considerable attention [e.g., *Easterling et al.*, 2000; *Allan and Soden*, 2008; *Rahmstorf and Coumou*, 2011; *Barriopedro et al.*, 2011; *Coumou and Rahmstorf*, 2012; *Palmer*, 2014; *Fischer and Knutti*, 2015]. After analyzing the frequency of extremely strong fronts we therefore assess the individual contributions of temperature and humidity to the change in the frequency of extremely strong fronts. This is important because the used front definition combines information on temperature and humidity gradients.

This study focuses on the question if the number of strong fronts changed during recent decades. We start with analyzing the annual number of extremely strong fronts, and then we identify their preferred season of occurrence and examine trends (section 3.1). Next we disentangle the individual contributions of moisture and temperature gradients to the observed trend (section 3.2). The analysis is repeated for a domain over North America (section 3.2). Finally, we discuss the relationship between frontal strength, frontal precipitation intensity, and implication of this relationship for extreme precipitation events (section 4) before we conclude.

2. Methods: Detection of Large-Scale Mobile Fronts and Attribution to Precipitation

We regard fronts as those types of large-scale mobile fronts that are associated with extratropical cyclones. The cyclone's cold and warm fronts separate air masses of different origin and character, e.g., warm-moist tropical air from cold-dry polar air. So far, meteorologist have not agreed on one ultimate definition of fronts [*Mass*, 1991; *Uccellini et al.*, 1992; *Sanders and Doswell*, 1995; *Hewson*, 1998; *Sanders*, 1999; *McCann and Whistler*, 2001], but several previous studies have identified θ_e as a powerful variable to detect large-scale mobile fronts due to its conservation properties [*Cahir and Lottes*, 1982; *Steinacker*, 1992; *Hewson*, 1997, 1998, 2009; *Jenkner et al.*, 2010; *Hewson and Titley*, 2010; *Berry et al.*, 2011; *Baldwin and Logsdon*, 2011]. Large-scale θ_e fronts are best identified at an elevated level, e.g., 850 hPa, to reduce the influence of diabatic processes at the surface (i.e., turbulent surface fluxes and boundary layer mixing), which can mask the character of the large-scale flow [*Renard and Clarke*, 1965; *Hewson*, 1998].

Because θ_e fronts combine the effect of strong humidity and temperature contrasts into one variable, a pure humidity gradient might be identified as a front. This can, however, be seen as an advantage, and *Lackmann* [2011] gave a practical example: during daytime differential heating on the cold and warm sides of a front acts to reduce the (potential) temperature gradient of the front. However, a zone of important weather activity can remain after the temperature front has vanished. In such a situation θ_e still detects a front, while a method based on potential temperature detects this front only at certain times during the day [*Lackmann*, 2011]. In addition, moisture gradients are important factors for the formation of deep convection, which is often related to the formation of strong precipitation events [*Sanders and Doswell*, 1995].

Following earlier studies [*Renard and Clarke*, 1965; *Clarke and Renard*, 1966; *Hewson*, 1998; *Jenkner et al.*, 2010; *Berry et al.*, 2011; *Schemm et al.*, 2015], fronts are identified at the 850 hPa level using the thermal front parameter. This parameter is defined as

$$\mathrm{TFP} \;=\; -\nabla|\nabla\theta_e|\cdot\nabla\theta_e/\,|\nabla\theta_e|$$

TFP (thermal front parameter) is a derivative of the magnitude of the θ_e gradient perpendicular to the frontal zone. The strength of a front is defined in terms of its θ_e gradient. Fronts are identified globally on a regular grid with 1° grid spacing. All quasi-stationary fronts, which, for example, form along coastlines, are removed from the data set by a minimum advection threshold of $3\,\mathrm{m\,s^{-1}}$ applied to the wind in the across-frontal direction. In addition, all fronts are required to have a minimum length of 500 km. A more detailed description, including validations and examples of the employed algorithm, is presented in *Schemm et al.* [2015]. This study is entirely based on 6-hourly ERA-Interim data [*Dee et al.*, 2011].

All front grid points are taken into account in our analyses. We do not assign one single value of the front strength to individual fronts. This increases the statistical robustness of our results, and it avoids difficulties when, for example, the front strength varies strongly along a front. Later, we compare the annual numbers of analyzed fronts and front grid points and show that our results are not a consequence of an increase in the number of fronts.

We further discuss the relationship between frontal strength and frontal precipitation. This relationship is evaluated using precipitation accumulated during the 6 h after frontal passage (t) and the frontal strength ($\mathrm{K\,[100\,km]^{-1}}$) at time t. Thus, at every grid point along a front, frontal gradients are associated with accumulated precipitation during the following 6 h. To account for the propagation of the front during these 6 h, precipitation rates are averaged in a radius of 300 km around the position of the frontal grid point at time t. An example that illustrates the method is given in Figure S1 in the supporting information. For consistency with the front data we also use the precipitation forecast data from ERA-Interim.

The total number of analyzed frontal grid points for Europe (10°W–25°E, 40–60°N) during the period January 1979–February 2014 is approximately 720,000, which corresponds to roughly 14 frontal grid points per 6-hourly time step.

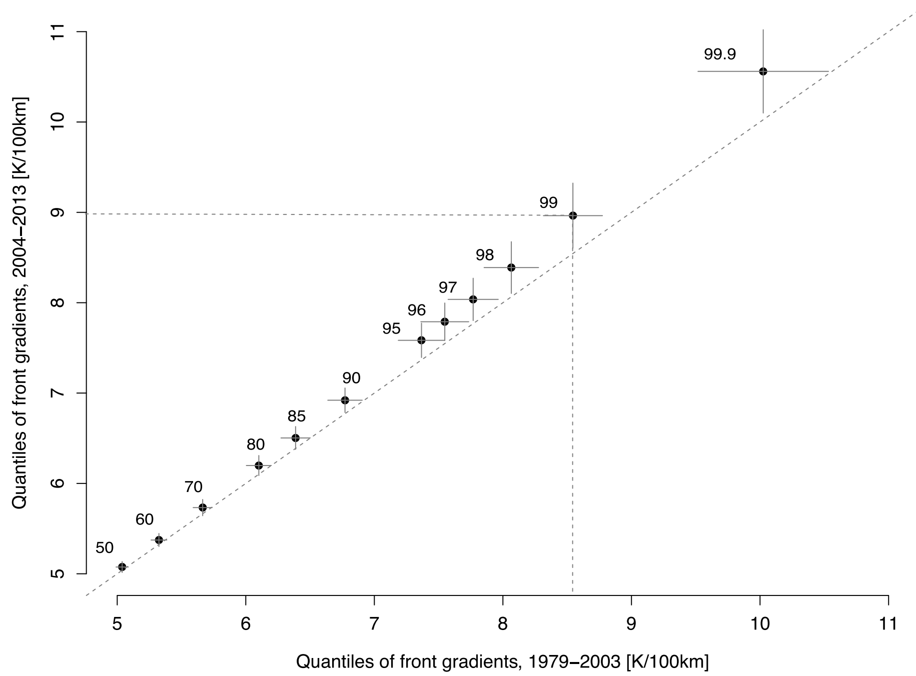

Figure 1. The quantile-quantile plot highlights the increase in extreme frontal strengths during recent years. Shown are the following quantiles calculated from all frontal grid points: 50–80 by 10, 85–95 by 5, 95–99 by 1, and 99.99 for the reference period 1979–2003 and the recent period 2004–2013. For example, the 99th percentile is 8.6 K [100 km]$^{-1}$ for the reference period, whereas for the recent period, it is 9.0 K [100 km]$^{-1}$. Additional gray lines at each dot span 2 times the standard deviation of the corresponding annually calculated percentile distribution for 1979–2003 (horizontal) and 2004–2013 (vertical). Considered are only fronts over Europe (10°W–25°E, 40–60°N).

3. Results

3.1. Increase in the Frequency of the Extremely Strong Fronts Over Europe

In Figure 1 the quantile-quantile plot of percentiles of frontal strength distributions over Europe (10°W–25°E, 40–60°N) for the period between January 2004 and December 2013 is compared to a reference period between 1979 and 2003. During this recent period the change is most pronounced. It reveals an increase in frontal strength for the percentiles above the 90th percentile. For example, the 99th percentile increased from 8.6 K [100 km]$^{-1}$ to 9.0 K [100 km]$^{-1}$ between the reference period (1979–2003) and the more recent period (2004–2013). This shift of the 99th percentile toward higher values exceeds the interannual variability of the 99th percentile in the reference period, which is indicated by the horizontal lines. Further, the relative frequency of having a gradient larger than 9 K [100 km]$^{-1}$ increased from 0.4% to 0.9% between, for example, the two recent decades 1991–2000 and 2001–2010. Hence, frontal strength has increased for all high quantiles (>90th percentile).

An analysis of the annual relative frequency of extremely strong fronts, i.e., fronts exceeding 10 K [100 km]$^{-1}$, indicates that their number has systematically increased over Europe during the past decades (Figure 2). A frontal strength exceeding 10 K [100 km]$^{-1}$ approximately corresponds to the 99.9th percentile of the frontal strength distribution, and these fronts are referred to as "extremely strong" or just "extreme." Fronts exceeding 9 K [100 km]$^{-1}$ are referred to as strong fronts and these also show an increase in their annual frequency (Figure S2). Annual relative frequencies are calculated by dividing the number of frontal grid points above the threshold by the total number of frontal grid points in the same year.

A logistic regression [*Frei and Schär*, 2001] reveals a statistically significant positive trend in the relative frequency of extreme frontal strengths (Figure 2). The logistic regression yields a *p* value of 0.0013, and the nonparametric Mann-Kendall test applied in combination with a Theil-Sen trend estimate yields a *p* value of 0.023. The increase is more pronounced after the year 2000. Finally, a seasonal analysis of frontal strengths (Figure S3) identifies summer (June–August (JJA)) and autumn (September–November (SON)) as the periods

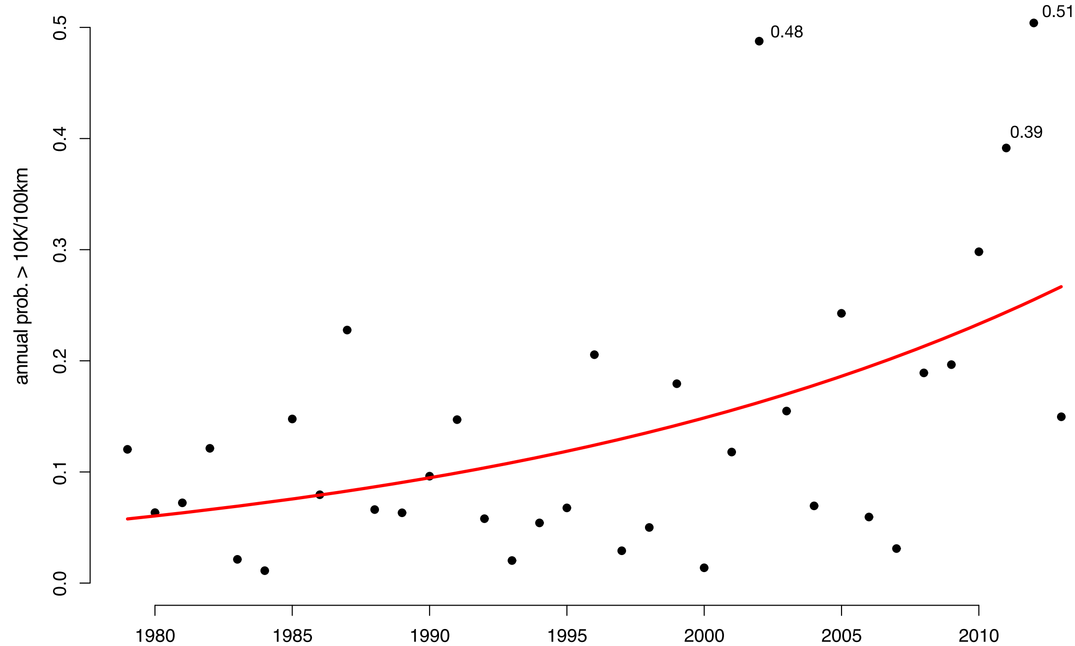

Figure 2. The annual relative frequency of occurrence of extreme frontal grid points, i.e., grid points with a front strength exceeding 10 K [100 km]$^{-1}$, shows a positive trend. The relative frequency is the number of frontal grid points above the threshold per year divided by the total number of fronts in a particular year. The red line shows a logistic regression fit. The estimated p value is 0.0013. The nonparametric Mann-Kendall test in combination with the Theil-Sen trend estimate yields a p value of 0.023. Hence, the increase in the number of extreme frontal strengths is statistically significant.

leading to the annual increases in the number of extremely strong fronts. During winter, the threshold for extreme fronts is rarely exceeded (Figure S3).

Next, consideration is given to the robustness of the result. First, there is no trend in the annual number of fronts or frontal grid points (Figure S4); therefore, the trend described above is not an artefact of an overall change of front frequency or length and is also observed in the annual absolute number of extreme fronts. As mentioned earlier, the trend in the frequency of extreme fronts remains statistically significant if the threshold is reduced from 10 K [100 km]$^{-1}$ (Figure 2) to 9 K [100 km]$^{-1}$ (Figure S2). The nonparametric Mann-Kendall test for the lower threshold yields a p value of 0.012 compared to 0.023 for the higher threshold. Second, for a single front, all frontal grid points above 10 K [100 km]$^{-1}$ are considered in the statistical analysis. Accordingly, the trend can potentially originate from a limited number of particularly strong and long fronts. However, even if the number of frontal grid points above the threshold is limited to one per time step per front, which ensures spatial independence of the strong frontal strengths, the trend is significant for the annual (Figure S5a) and the JJA rates (Figure S5b). Third, regarding the quality of the employed reanalysis product, a thorough comparison of trends in humidity and surface temperature over Europe showed a high agreement between ERA-Interim and an independent observation-based data set [*Simmons et al.*, 2010]. We also note that the trend is weaker during earlier decades than the one analyzed (2004–2013).

Finally, we note that extremely strong fronts can occur at various places over Europe (Figure S6). Regions where frontal strength frequently exceeds 10 K [100 km]$^{-1}$ encompass mountainous regions such as the western Alps, the Dinaric Alps (19.5°W, 42°N), the Scandinavian mountains in southwestern Norway, and the Cantabrian mountains in northwestern Spain, as well as the west coast of Ireland and also many parts of France, northern Germany, Denmark, and the Baltic Sea with lower topography (Figure S6). This suggests that fronts that trail synoptic-scale depressions reach extreme strength frequently but not solely after making landfall or during interaction with steep orography.

3.2. Change in Frontal Strength: Moisture or Temperature Gradients as Main Driver?

Next, we are interested in the processes that result in this trend. Frontal strength, as analyzed in this study, is a function of across-frontal temperature and specific humidity gradients; therefore, changes in either of the two or both quantities can drive the observed trend in frontal strength. In the hypothetical case of uniform warming on both sides of a saturated front, the specific humidity increase will be more pronounced on the warm side of the front than on the cold side, because saturation water vapor pressure increases nonlinearly with temperature. Consequently, the frontal humidity gradient would increase, while the temperature gradient remains constant.

To shed light on the driving variable of the trend, we first consider the gradient of specific humidity for strong front grid points ($9\,\mathrm{K}\,[100\,\mathrm{km}]^{-1}$), calculated on an annual basis (Figure 3a). All four examined percentiles of the specific humidity gradient (25th, 50th, 75th, and 95th) exhibit an upward trend. This upward trend is statistically significant for the 25th (p value ~ 0.003) and the 95th percentiles (p value ~ 0.04), it is weakly significant for the median (p value ~ 0.08), and not significant for the 75th percentile. Next, we consider the gradient of temperature for strong front grid points (Figure 3b). Here the percentiles show a nonsignificant weak decrease (the estimated p value for the median and the 95th percentile is 0.2 and even larger for the 25th and the 75th percentiles). Based on these findings, we argue that the trend in the number of strong and extremely strong fronts is primarily driven by increasing atmospheric humidity. This is further supported by the fact that the annual median of specific humidity along strong fronts shows an upward trend in the ERA-Interim as well as in the Modern-Era Retrospective Analysis for Research and Applications (MERRA) [*Rienecker et al*., 2011] data sets (Figure S7). Our findings are consistent with (i) the fact that most extreme fronts are identified during JJA, when atmospheric humidity is higher than in the other seasons, and (ii) the observed increase in humidity over Europe in the considered period [*Intergovernmental Panel on Climate Change (IPCC)*, 2013].

However, low-tropospheric humidity is not increasing on all continents. For example, humidity trends over most parts of the U.S. are weak and close to zero and, most importantly, are not statistically significant [*IPCC*, 2013, Figure 2.30]. We therefore examine the occurrence of trends in the number of extreme fronts also over North America, in a region with, in contrast to Europe, insignificant humidity trends. The region encompasses the U.S. and southern Canada east of the Rocky Mountains (110–60°W, 30°–60°N). In contrast to Europe we find in this region no upward trend in the number of extreme fronts (Figure S8). Hence, this result corroborates the important role of humidity as the driver for the identified increase in the number of extreme fronts over Europe.

4. Discussion: Frontal Strength and Implications for Frontal Precipitation

Observed trends in summertime extreme precipitation in Europe are characterized by a pronounced spatial variability and can even have opposite signs in adjacent regions [*Moberg and Jones*, 2005; *Moberg et al*., 2006; *Zolina et al*., 2008, 2009; *Scherrer et al*., 2016]. For example, for the summer season *Zolina et al*. [2005] report negative trends for the Netherlands and Denmark, mixed trends over eastern Europe, and positive trends in the Alpine region. For Europe several studies suggest an increase in the likelihood of extreme summer precipitation events [*Christensen and Christensen*, 2003; *Huntingford et al*., 2003; *Giorgi et al*., 2016] despite the overall summertime drying trend over central and western Europe [*Pal et al*., 2004]. To better understand this complex trend behavior, we argue that changes in the dynamic and thermodynamic properties of individual weather systems, as demonstrated in this study for fronts, may turn out to be key.

Considering the relationship between frontal strength and precipitation for Europe (10°W–25°E, 40–60°N), we find that with increasing frontal strength the frontal precipitation rate also becomes stronger (Figure 4). The increase is more pronounced in the mean and in the interquantile (25%–75%) range compared to the median values and is strongest for the 95th percentile of frontal precipitation. This is in agreement with the findings of *Catto and Pfahl* [2013] who note that extreme-precipitation-producing fronts have up to 35% stronger frontal strengths. This implies that an increase in the number of extremely strong fronts (Figures 1 and 2) potentially is one driving agent behind an increase in the number of extreme precipitation events, in particular, because summertime convective thunderstorms frequently form in prefrontal zones [*Browning and Monk*, 1982; *van Delden*, 1998, 2001; *Dahl and Fischer*, 2016].

Furthermore, the findings suggest that regionally varying trends in precipitation can potentially be driven by the spatial variability in the frequency of strong and extremely strong fronts. Our findings indicate that

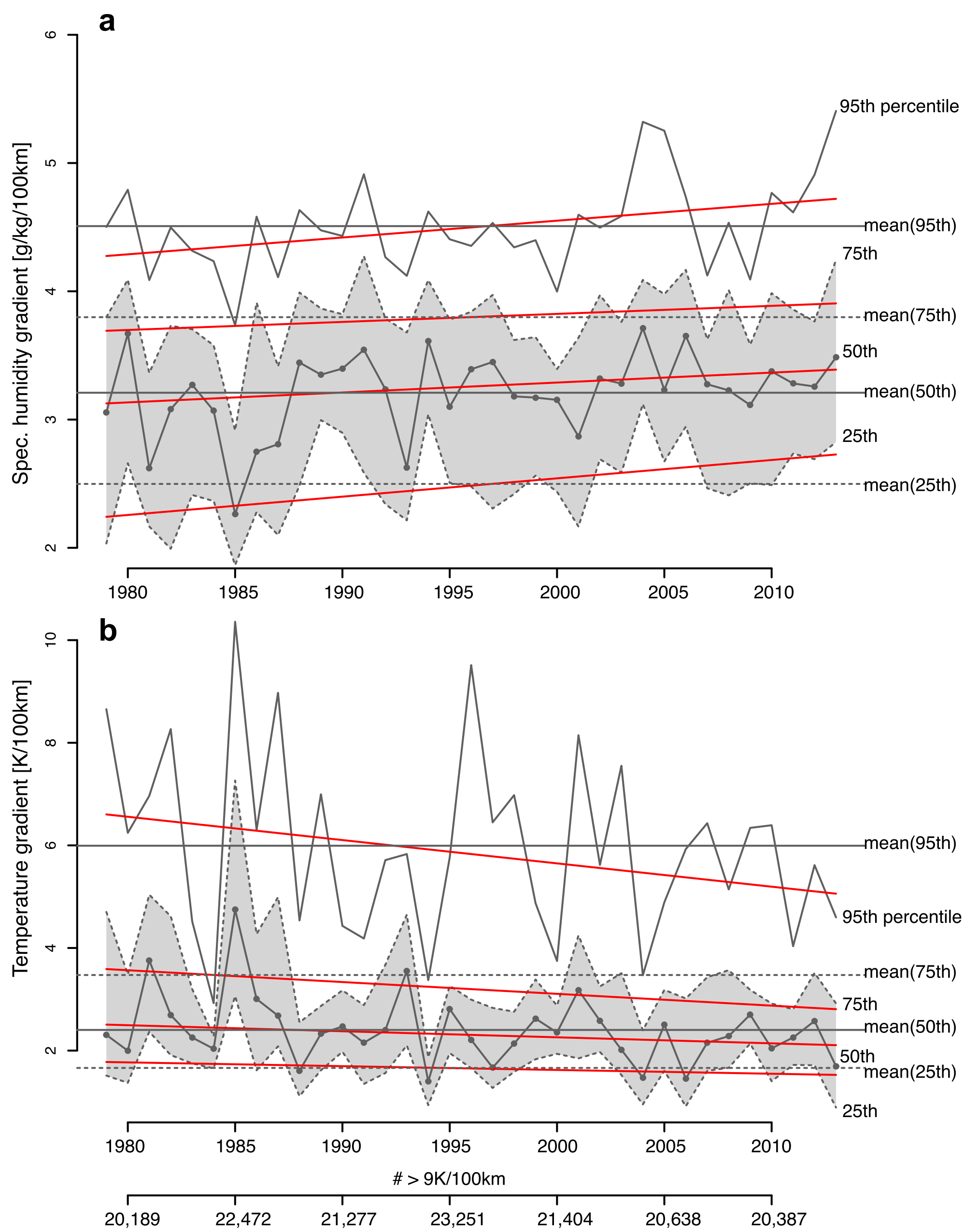

Figure 3. Shown are the annual 25th (dashed), 50th (thick solid, black dots), 75th (dashed), and 95th (solid) percentiles of (a) specific humidity and (b) temperature gradients across strong fronts (frontal strength exceeding 9 K $[100\,km]^{-1}$). The interquantile range is shaded gray. Black lines show the mean for each percentile over the entire time period. Trend estimates as obtained from the nonparametric Mann-Kendall test in combination with the Theil-Sen slope estimate for each percentile are shown in red; they are not significant for the temperature gradients but are so for 25th, 50th, and the 95th percentiles of the specific humidity gradients (see text for *p* values). Additionally shown are the numbers of frontal grid points exceeding 9 K $[100\,km]^{-1}$ in 5 year intervals.

there is a need for, and potential in, future research to address the linkage between changes in the dynamic properties of weather systems, for example, fronts, and the associated regional variability of extreme precipitation events.

Over North America, where no trend in the number of extremely strong fronts is identified, *Kunkel et al*. [2013] report mixed precipitation trends. Trends are significant in the Southeast and Midwest but not significant in the Northeast and over the Northern Great Plains.

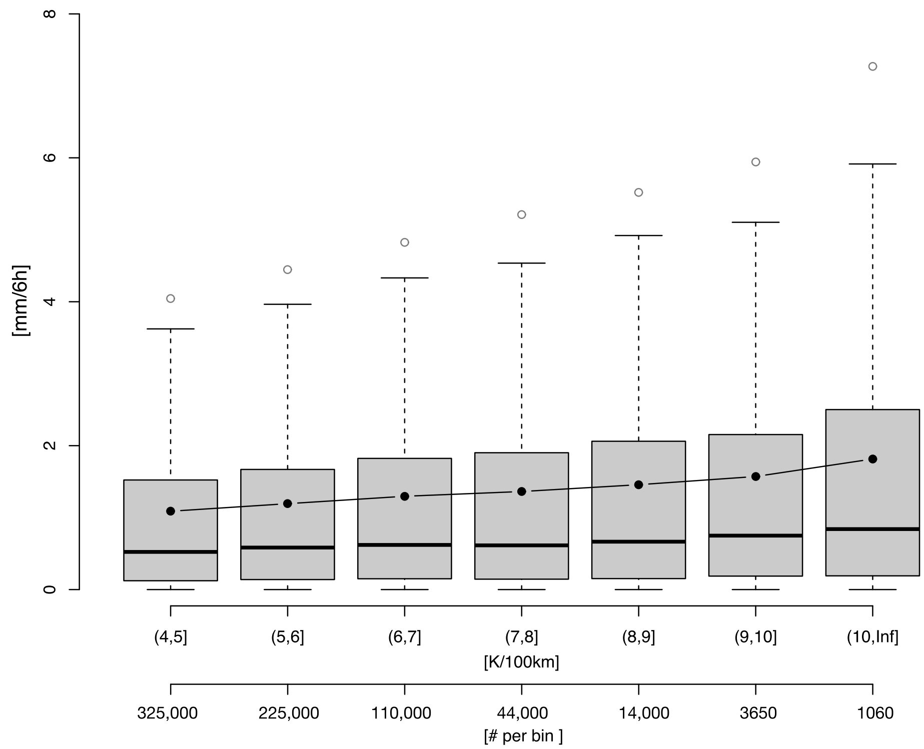

Figure 4. Frontal strength and its relationship with frontal precipitation: The box-and-whisker diagram indicates an increase in mean frontal precipitation (mm [6 h]$^{-1}$) with increasing frontal strength (K [100 km]$^{-1}$). For each category of frontal strength, the mean (black solid filled circles) and median (horizontal black line) is shown. Whiskers span 1.5 times the interquantile range (25%–75%) indicated by the gray box. Open circles indicate the 95th percentile of each category. The number of members in each category is listed along the bottom axis. Gamma fit parameters are given in the text.

Finally, we note that the fact that frontal precipitation increases with stronger θ_e gradients is solely a consequence of an increase in humidity and also due to more intense frontal dynamics. The forcing of vertical motion can be quantified using the Q-vector convergence [*Hoskins et al.*, 1978; *Barnes*, 1985; *Keyser et al.*, 1988; *Davies*, 2015]. Q-vectors computed at 850 hPa and attributed to the 850 hPa frontal strength, suggest stronger Q-vector convergence with increasing frontal strength (Figure S9). This implies that the increase of frontal precipitation with frontal strength is both an effect of increased frontal dynamics (frontogenesis) and increased humidity.

5. Conclusions

We have argued in this study, based on analyses of atmospheric reanalysis data and using a front definition based on equivalent potential temperature at 850 hPa, that the number of extremely strong fronts over Europe has increased over the past decades due to an increase in specific humidity gradients. This trend appears to be robust for Europe, and its absence over North America is noteworthy. We argue that the contrasting trend in the number of extreme fronts is driven by the differing humidity trends over Europe and North America. Humidity gradients are known to be an important factor for the formation of deep convection [*Sanders and Doswell*, 1995]. Indeed, we further showed, for Europe, that frontal precipitation increases with frontal strength. Hence, the upward trend in the number of strong fronts potentially can help to explain the observed regional variations in extreme precipitation over Europe [*Zolina et al.*, 2014; *Murawski et al.*, 2015]. Note, however, that frontal storms are only one scenario for extreme precipitation in summer. Yet our findings highlight the importance of changes in the dynamic and thermodynamic properties of synoptic-scale weather systems (here low-tropospheric fronts), which in turn may act as drivers for the regional variability of high-impact weather (e.g., intense precipitation).

Acknowledgments
We would like to thank Christoph Frei from MeteoSwiss, who kindly provided the R packages [*R Core Team. R*, 2014] used in this study to perform the Mann-Kendall and Theil-Sen trend estimates. The MERRA data used in this study were provided by the Global Modeling and Assimilation Office (GMAO) at NASA Goddard Space Flight Center through the NASA GES DISC online archive. The authors also acknowledge ECMWF for providing the ERA-Interim reanalysis data set, which is available via the ECMWF online archive. The monthly mean front data are publicly available at http://eraiclim.ethz.ch, and fronts at higher temporal resolution are available on request from the corresponding author (sebastian.schemm@uib.no). Sebastian Schemm acknowledges funding from the Swiss National Science Foundation (P300P2_167745) and from the State Environmental Agency Rhineland-Palatinate, Mainz, Germany. We acknowledge two anonymous reviewers for their constructive comments.

References

Allan, R. P., and B. J. Soden (2008), Atmospheric warming and the amplification of precipitation extremes, *Science*, *321*, 1481–1484.

Baldwin, M., and J. Logsdon (2011), Incorporation of forcing characteristics into a prediction system for high-impact convective precipitation events, COMET Partners Project Final Report, UCAR Award No.: Z10-83406. [Available at http://www.comet.ucar.edu/outreach/abstract_final/1083406.htm.]

Barnes, S. L. (1985), Omega diagnostics as a supplement to LFM/MOS guidance in weakly forced convective situations, *Mon. Weather Rev.*, *113*, 2122–2141.

Barriopedro, D., E. M. Fischer, J. Luterbacher, R. M. Trigo, and R. García-Herrera (2011), The hot summer of 2010: Redrawing the temperature record map of Europe, *Science*, *332*, 220–224.

Berry, G., M. J. Reeder, and C. Jakob (2011), A global climatology of atmospheric fronts, *Geophys. Res. Lett.*, *38*, L04809, doi:10.1029/2010GL046451.

Browning, K. A., and G. A. Monk (1982), A simple model for the synoptic analysis of cold fronts, *Q. J. R. Meteorol. Soc.*, *108*, 435–452.

Cahir, J. J., and W. D. Lottes (1982), An objective diagnostic aid in locating meteorologically significant boundaries, in *Preprints of 9th Conference on Weather Forecasting and Analysis, Seattle, Washington, June 28–July 1, 1982*, pp. 296–299, Am. Meteorol. Soc., Boston.

Catto, J. L., and S. Pfahl (2013), The importance of fronts for extreme precipitation, *J. Geophys. Res. Atmos.*, *118*, 10,791–10,801, doi:10.1002/jgrd.50852.

Catto, J. L., C. Jakob, G. Berry, and N. Nicholls (2012), Relating global precipitation to atmospheric fronts, *Geophys. Res. Lett.*, *39*, L10805, doi:10.1029/2012GL051736.

Christensen, J. H., and O. B. Christensen (2003), Climate modelling: Severe summertime flooding in Europe, *Nature*, *6925*, 805–806, doi:10.1038/421805a.

Clarke, L. C., and R. J. Renard (1966), The U.S. Navy numerical frontal analysis scheme: Further development and a limited evaluation, *J. Appl. Meteorol.*, *5*, 764–777.

Coumou, D., and S. Rahmstorf (2012), A decade of weather extremes, *Nat. Clim. Change*, *2*, 491–496.

Dahl, J. M. L., and J. Fischer (2016), The origin of western European warm-season prefrontal convergence lines, *Weather Forecast.*, *31*, 1417–1431, doi:10.1029/2004GL019836.

Davies, H. C. (2015), The quasigeostrophic omega equation: Reappraisal, refinements, and relevance, *Mon. Weather Rev.*, *143*, 3–25.

Dee, D. P., et al. (2011), The ERA-Interim reanalysis: Configuration and performance of the data assimilation system, *Q. J. R. Meteorol. Soc.*, *137*, 553–597.

Easterling, D. R., J. L. Evans, P. Y. Groisman, T. R. Karl, K. E. Kunkel, and P. Ambenje (2000), Observed variability and trends in extreme climate events: A brief review, *Bull. Am. Meteorol. Soc.*, *81*, 417–425.

Fischer, E. M., and R. Knutti (2015), Anthropogenic contribution to global occurrence of heavy-precipitation and high-temperature extremes, *Nat. Clim. Change*, *5*, 560–564.

Frei, C., and C. Schär (2001), Detection probability of trends in rare events: Theory and application to heavy precipitation in the Alpine region, *J. Clim.*, *14*, 1568–1584.

Giorgi, F., C. Torma, E. Coppola, N. Ban, C. Schär, and S. Somot (2016), Enhanced summer convective rainfall at Alpine high elevations in response to climate warming, *Nat. Geosci.*, *9*, 584–589.

Hewson, T. D. (1997), Objective identification of frontal wave cyclones, *Met. Apps.*, *4*, 311–315.

Hewson, T. D. (1998), Objective fronts, *Met. Apps*, *5*, 37–65.

Hewson, T. D. (2009), Diminutive frontal waves—A link between fronts and cyclones, *J. Atmos. Sci.*, *66*, 116–132.

Hewson, T. D., and H. Titley (2010), Objective identification, typing and tracking of the complete life-cycles of cyclonic features at high spatial resolution, *Met. Apps.*, *17*, 355–381.

Hoskins, B. J., I. Draghici, and H. C. Davies (1978), A new look at the *w*-equation, *Q. J. R. Meteorol. Soc.*, *104*, 31–38.

Huntingford, C., R. G. Jones, C. Prudhomme, R. Lamb, J. H. C. Gash, and D. A. Jones (2003), Regional climate model predictions of extreme rainfall for a changing climate, *Q. J. R. Meteorol. Soc.*, *129*, 1607–1622.

Intergovernmental Panel on Climate Change (IPCC) (2013), Observations: Atmosphere and surface, in *Climate Change 2013: The Physical Science Basis. Contribution of Working Group I to the Fifth Assessment Report of the Intergovernmental Panel on Climate Change*, edited by T. F. Stocker et al., Cambridge Univ. Press, Cambridge, U. K., and New York.

James, P. K., and K. A. Browning (1979), Mesoscale structure of line convection at surface cold fronts, *Q. J. R. Meteorol. Soc.*, *105*, 371–382.

Jenkner, J. M., M. Sprenger, I. Schwenk, C. Schwierz, S. Dierer, and D. Leuenberger (2010), Detection and climatology of fronts in a high-resolution model reanalysis over the Alps, *Met. Apps.*, *17*, 1–8.

Keyser, D., M. J. Reeder, and R. J. Reed (1988), A generalization of Petterssen's frontogenesis function and its relation to the forcing of vertical motion, *Mon. Weather Rev.*, *116*, 762–780.

Kunkel, K. E., et al. (2013), Monitoring and understanding trends in extreme storms, *Bull. Am. Meteorol. Soc.*, *94*, 499–514.

Lackmann, G. (2011), *Midlatitude Synoptic Meteorology: Dynamics, Analysis and Forecasting*, pp. 345, Am. Meteorol. Soc., Massachusetts.

Mass, C. (1991), Surface synoptic analysis: Time for a reassessment?, *Bull. Am. Meteorol. Soc.*, *72*, 348–363.

McCann, D. W., and J. P. Whistler (2001), Problems and solutions for drawing fronts objectively, *Met. Apps*, *8*, 195–203.

Mills, G. A. (2005), A re-examination of the synoptic and mesoscale meteorology of Ash Wednesday 1983, *Aust. Meteorol. Mag.*, *54*, 35–55.

Moberg, A., and P. D. Jones (2005), Trends in indices for extremes in daily temperature and precipitation in central and western Europe, 1901–99, *Int. J. Climatol.*, *25*, 1149–1171.

Moberg, A., et al. (2006), Indices for daily temperature and precipitation extremes in Europe analyzed for the period 1901–2000, *J. Geophys. Res.*, *111*, D22106, doi:10.1029/2006JD007103.

Murawski, A., J. Zimmer, and B. Merz (2015), High spatial and temporal organization of changes in precipitation over Germany for 1951–2006, *Int. J. Climatol.*, *36*, 2582–2597.

Pal, J. S., F. Giorgi, and X. Bi (2004), Consistency of recent European summer precipitation trends and extremes with future regional climate projections, *Geophys. Res. Lett.*, *31*, L13202, doi:10.1029/2004GL019836.

Palmer, T. (2014), Record-breaking winters and global climate change, *Science*, *344*, 803–804.

R Core Team. R (2014), *A Language and Environment for Statistical Computing*, R Foundation for Statistical Computing, Vienna, Austria. [Available at http://www.R-project.org.]

Rahmstorf, S., and D. Coumou (2011), Increase of extreme events in a warming world, *Proc. Natl. Acad. Sci. U.S.A.*, *108*, 17,905–17,909.

Reeder, M. J., T. Spengler, and R. Musgrave (2015), Rossby waves, extreme fronts, and wildfires in southeastern Australia, *Geophys. Res. Lett.*, *42*, 2015–2023, doi:10.1002/2015GL063125.

Renard, R., and L. Clarke (1965), Experiments in numerical objective frontal analysis, *Mon. Weather Rev.*, *93*, 547–556.
Rienecker, M. M., et al. (2011), MERRA, NASA's Modern-Era Retrospective Analysis for Research and Applications, *J. Clim.*, *24*, 3624–3648.
Sanders, F. (1999), A proposed method of surface map analysis, *Mon. Weather Rev.*, *127*, 945–955.
Sanders, F., and C. A. Doswell III (1995), A case for detailed surface analysis, *Bull. Am. Meteorol. Soc.*, *76*, 505–521.
Schemm, S., I. Rudeva, and I. Simmonds (2015), Extratropical fronts in the lower troposphere—Global perspectives obtained from two automated methods, *Q. J. R. Meteorol. Soc.*, *141*, 1686–1698.
Schemm, S., L. Nisi, A. Martynov, D. Leuenberger, and O. Martius (2016), On the link between cold fronts and hail in Switzerland, *Atmos. Sci. Lett.*, *12*, 315–325.
Scherrer, S., E. M. Fischer, R. Posselt, M. A. Liniger, M. Croci-Maspoli, and R. Knutti (2016), Emerging trends in heavy precipitation and hot temperature extremes in Switzerland, *J. Geophys. Res. Atmos.*, *121*, 2626–2637, doi:10.1002/2015JD024634.
Simmons, A. J., K. M. Willett, P. D. Jones, P. W. Thorne, and D. P. Dee (2010), Low- frequency variations in surface atmospheric humidity, temperature, and precipitation: Inferences from reanalyses and monthly gridded observational data sets, *J. Geophys. Res.*, *115*, D01110, doi:10.1029/2009JD012442.
Steinacker, R. A. (1992), Dynamic aspects of frontal analysis, *Meteorol. Atmos. Phys.*, *48*, 93–103.
Uccellini, L. W., S. F. Corfidi, N. W. Junker, P. J. Kocin, and D. A. Olson (1992), Report on the surface analysis workshop at the National Meteorological Center 25–28 March 1991, *Bull. Am. Meteorol. Soc.*, *73*, 459–471.
van Delden, A. (1998), The synoptic setting of a thundery low and associated prefrontal squall line in western Europe, *Meteorol. Atmos. Phys.*, *65*, 113–131.
van Delden, A. (2001), The synoptic setting of thunderstorms in western Europe, *Atmos. Res.*, *56*, 89–110.
Volkert, H., L. Weickmann, and A. Tafferner (1987), The papal front of 3 May 1987—A remarkable example of frontogenesis near the Alps, *Q. J. R. Meteorol. Soc.*, *117*, 125–150.
Zolina, O., C. Simmer, A. Kapala, and S. Gulev (2005), On the robustness of the estimates of centennial-scale variability in heavy precipitation from station data over Europe, *Geophys. Res. Lett.*, *32*, L14707, doi:10.1029/2005GL023231.
Zolina, O., C. Simmer, A. Kapala, S. Bachner, S. Gulev, and H. Maechel (2008), Seasonally dependent changes of precipitation extremes over Germany since 1950 from a very dense observational network, *J. Geophys. Res.*, *113*, D06110, doi:10.1029/2007JD008393.
Zolina, O., C. Simmer, K. Belyaev, A. Kapala, and S. Gulev (2009), Improving estimates of heavy and extreme precipitation using daily records from European rain gauges, *J. Hydrometeorol.*, *10*, 701–716.
Zolina, O., C. Simmer, A. Kapala, P. Shabanov, P. Becker, H. Mächel, S. Gulev, and P. Groisman (2014), Precipitation variability and extremes in central Europe: New view from STAMMEX results, *Bull. Am. Meteorol. Soc.*, *95*, 995–1002.